A Trust Region Aggressive Space Mapping Algorithm for EM Optimization

Mohamed H. Bakr, *Student Member, IEEE*, John W. Bandler, *Fellow, IEEE*, Radoslaw M. Biernacki, *Fellow, IEEE*, Shao Hua (Steve) Chen, *Senior Member, IEEE*, and Kaj Madsen

Abstract—A robust new algorithm for electromagnetic (EM) optimization of microwave circuits is presented. The algorithm (TRASM) integrates a trust region methodology with the aggressive space mapping (ASM). The trust region ensures that each iteration results in improved alignment between the coarse and fine models needed to execute ASM. The parameter extraction step is a crucial part of the ASM technique. The nonuniqueness of this step may result in the divergence of the technique. To improve the uniqueness of the extraction phase, we developed a recursive multipoint parameter extraction. This suggested step exploits all the available EM simulations for improving the uniqueness of parameter extraction. The new algorithm was successfully used to design a number of microwave circuits. Examples include the EM optimization of a double-folded stub filter and of a high-temperature superconducting (HTS) filter using Sonnet's *em*. The proposed algorithm was also used to design two-section, three-section, and seven-section waveguide transformers exploiting Maxwell Eminence. The design of a three-section waveguide transformer with rounded corners was carried out using HP HFSS. We show how the mapping can be used to carry out Monte Carlo analysis using only coarse model simulations.

Index Terms—CAD, electromagnetic simulation, Monte Carlo analysis, microwave filters, optimization methods, space mapping.

I. INTRODUCTION

A NOVEL algorithm for aggressive space mapping (ASM) optimization [1] is introduced. Space mapping aims at aligning two different simulation models: a "coarse" model, typically an empirical circuit simulation, and a "fine" model, typically a full-wave EM simulation. The technique combines the accuracy of the fine model with the speed of the coarse model. Parameter extraction is a crucial part of the technique. In this step the parameters of the coarse model whose re-

sponses match the fine model responses are obtained. The extracted parameters may not be unique, causing the technique to fail to converge.

Recently, a multipoint parameter extraction concept was proposed [2] to enhance the uniqueness of the extraction step at the expense of an increased number of fine model simulations. The selection of points was arbitrary, not automated, and no information about the mapping between the two spaces was taken into account.

Our proposed trust region aggressive space mapping (TRASM) algorithm automates the selection of fine model points used for the multipoint parameter extraction process. In the multipoint parameter extraction, an iterative approach utilizes all the fine model points simulated since the last successful iteration. Also, the current approximation to the mapping between the two spaces is integrated into the parameter extraction step. The space mapping step at each iteration is constrained by a suitable trust region [3].

The TRASM algorithm was applied to a number of examples. The EM solver *em*[1] was used successfully to optimize the design of a high-temperature superconducting (HTS) filter and a double-folded stub filter. Maxwell Eminence[2] through Empipe3D[3] was used as a fine model to design two-section, three-section, and seven-section waveguide transformers. HP HFSS[4] was used to carry out the optimization of a three-section waveguide transformer with rounded corners. The coarse models for these examples exploited either a coarse grid EM model or circuit-theoretic/analytical models. The different types of models used illustrate the flexibility of selection of coarse and fine models.

The required number of fine model simulations to obtain the final design, as demonstrated by the examples, is of the order of the problem dimension. Such designs would otherwise be obtained by computationally very expensive direct optimizations of the fine models.

The algorithm also establishes a mapping between the two spaces, the fine model space and the coarse model space. This mapping is updated at each iteration of the algorithm. The final mapping can be used to carry out a space-mapped Monte

[1] *em* is a trademark of Sonnet Software, Inc., Liverpool, NY 13088 USA.

[2] *Maxwell Eminence* is a trademark of Ansoft Corporation, Pittsburgh, PA 15219 USA.

[3] *OSA90/hope*, *Empipe*, and *Empipe3D* are trademarks of the former Optimization Systems Associates Inc., Dundas, Ont., Canada, L9H 5E7, now HP EEsof Division, Santa Rosa, CA 95403 USA.

[4] *HP HFSS* is a trademark of HP EEsof Division, Santa Rosa, CA 95403 USA.

Carlo analysis of the fine model exploiting only coarse model simulations. We demonstrate this approach by performing a statistical analysis of the three-section waveguide transformer with rounded corners simulated by HP HFSS.

II. THE AGGREGATIVE SPACE MAPPING TECHNIQUE

It is assumed that the circuit under consideration can be simulated using two models: a fine model and a coarse model. The fine model is accurate but is computationally intensive. This model can, for example, be a finite element model. We refer to the vector of parameters of this model as x_{em}. The coarse model is a fast model but it is less accurate than the fine model. This model can be a circuit-theoretic empirical model. The vector of parameters of this model is referred to as x_{os}.

The first step of the technique is to obtain the optimal design of the coarse model x_{os}^*. The technique aims at establishing a mapping P between the two spaces [1]

$$x_{os} = P(x_{em}) \tag{1}$$

such that

$$\|R_{em}(x_{em}) - R_{os}(x_{os})\| \le \varepsilon \tag{2}$$

where R_{em} is the vector of fine model responses, R_{os} is the vector of coarse mode responses, and $\| \; \|$ is a suitable norm. The error function

$$f = P(x_{em}) - x_{os}^* \tag{3}$$

is first defined. The final fine-model design is obtained and the mapping is established if a solution for the system of nonlinear equations

$$f(x_{em}) = 0 \tag{4}$$

is found.

Let $x_{em}^{(i)}$ be the ith iterate in the solution of (4). The next iterate $x_{em}^{(i+1)}$ is found by a quasi-Newton iteration

$$x_{em}^{(i+1)} = x_{em}^{(i)} + h^{(i)} \tag{5}$$

where $h^{(i)}$ is obtained from

$$B^{(i)} h^{(i)} = -f\left(x_{em}^{(i)}\right) \tag{6}$$

and $B^{(i)}$ is an approximation to the Jacobian of the vector f with respect to x_{em} at the ith iteration. The matrix B is updated at each iteration using Broyden's update [4].

It is clear from (1)–(3) that the vector function f is obtained by evaluating $P(x_{em})$. This can be achieved through the process of parameter extraction. This extraction step involves solving a subsidiary optimization problem. The parameter extraction step is discussed in more detail in Section III.

III. THE PARAMETER EXTRACTION STEP

In the parameter extraction step, the parameters of the coarse model whose response matches the fine model response are obtained. It can be formulated as

$$\underset{x_{os}}{\text{minimize}} \left\| R_{em}\left(x_{em}^{(i)}\right) - R_{os}(x_{os}) \right\|. \tag{7}$$

The extracted parameters may not be unique, causing the technique to fail to converge.

A multipoint parameter extraction concept was proposed [2] to enhance the uniqueness of parameter extraction at the expense of an increased number of fine-model simulations. This extraction step is given by

$$\underset{x_{os}}{\text{minimize}} \| R_{os}(x_{os} + \Delta x) - R_{em}(x_{em} + \Delta x) \| \tag{8}$$

simultaneously for a set of perturbations Δx. Thus, the two models are matched at a number of points. In [2], there were no guidelines regarding the selection or the number of points used for the multipoint parameter extraction. Also, there is one important drawback in the multipoint parameter extraction procedure suggested in [2]. It was assumed that the perturbation Δx is identical in both spaces. This is not reliable since the relation between the perturbations in the two spaces is determined by the matrix B, which is an approximation of the Jacobian of the coarse-model parameters with respect to the fine-model parameters, not by the identity matrix. Our new algorithm automates the selection of fine-model points used for the multipoint parameter extraction. This new algorithm is presented in the next section.

IV. THE TRASM NEW ALGORITHM

At the ith iteration, the residual vector $f^{(i)} = P(x_{em}^{(i)}) - x_{os}^*$ defines the difference between the vector of extracted coarse model parameters $x_{os}^{(i)} = P(x_{em}^{(i)})$ and the optimal coarse model design. The mapping between the two models is established if this residual vector is driven to zero. It follows that the value $\|f^{(i)}\|$ can serve as a measure of the misalignment between the two spaces in the ith iteration. The step taken in the ith iteration is obtained from

$$\left(B^{(i)T}B^{(i)} + \lambda I\right)h^{(i)} = -B^{(i)T}f^{(i)} \tag{9}$$

where $B^{(i)}$ is an approximation to the Jacobian of the coarse-model parameters with respect to the fine-model parameters at the ith iteration. The parameter λ is selected such that the step obtained satisfies $\|h^{(i)}\| \le \delta$, where δ is the size of the trust region. This is done by utilizing the iterative algorithm suggested in [3]. The point suggested for the next iteration is $x_{em}^{(i+1)} = x_{em}^{(i)} + h^{(i)}$. Single-point parameter extraction is then applied at the point $x_{em}^{(i+1)}$ to get $f^{(i+1)} = P(x_{em}^{(i+1)}) - x_{os}^*$. The point $x_{em}^{(i+1)}$ is accepted and the matrix $B^{(i)}$ is updated using Broyden's formula [4] if a success criterion related to the reduction in the l_2 norm of the vector f is satisfied. In our
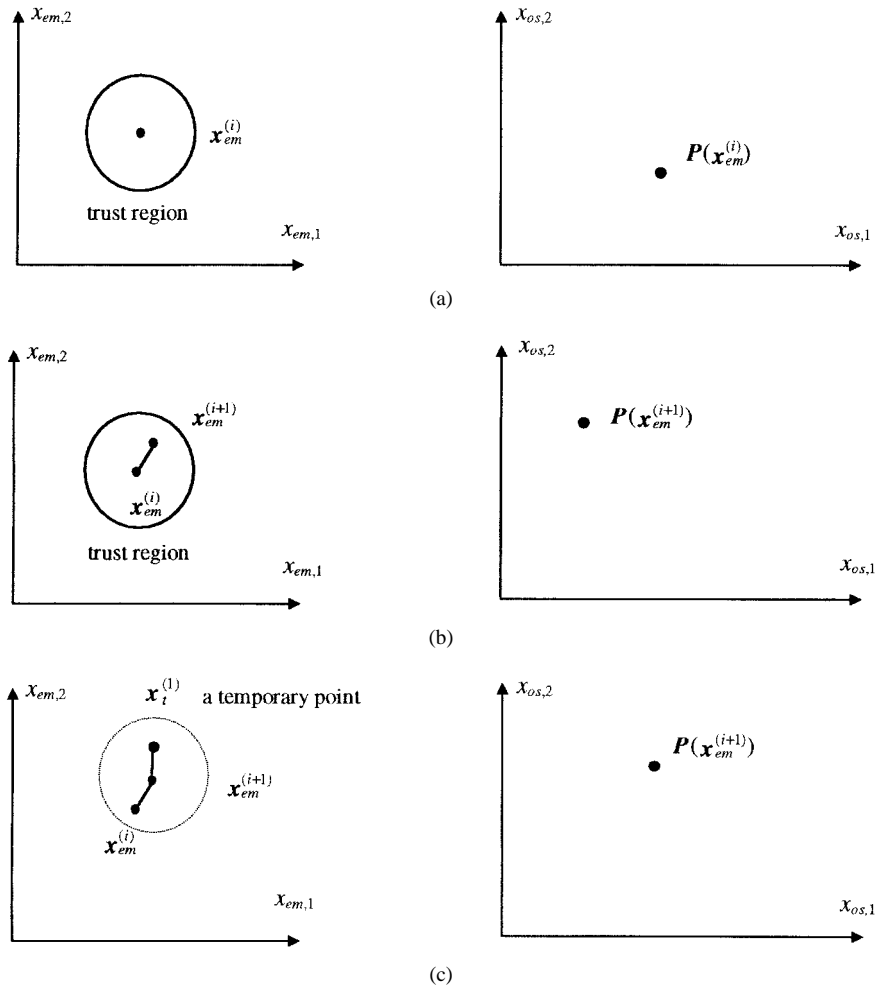
Fig. 1. Illustration of the automated multipoint parameter extraction. (a) The current state at the ith iteration. (b) Initial parameter extraction at the suggested point X_{em}^{i+1}. (c) Parameter extraction fails; an additional point X_t^1 is obtained and multipoint parameter extraction is carried out to sharpen the solution.

implementation, this success criterion is given by

$$\left(\left\|f^{(i)}\right\| - \left\|f^{(i+1)}\right\|\right) \geq 0.01\left(\left\|f^{(i)}\right\| - \left\|f^{(i)} + B^{(i)}h^{(i)}\right\|\right). \tag{10}$$

The success criterion (10) ensures that the ratio between the actual reduction in the l_2 norm of the vector f and the predicted reduction is greater than a certain value. Otherwise, the validity of the extraction process leading to $f^{(i+1)}$ at the suggested point $x_{em}^{(i+1)}$ is suspect. The residual vector $f^{(i+1)}$ is then used to construct a candidate point from the point $x_{em}^{(i+1)}$ by using (9). This candidate point is then added to the set of points employed for simultaneous parameter extraction at the point $x_{em}^{(i+1)}$. A new value for $f^{(i+1)}$ is obtained by solving

$$\underset{x_{os}}{\text{minimize}} \left\|R_{os}\left(x_{os} + B^{(i)}\left(x_{em} - x_{em}^{(i+1)}\right)\right) - R_{em}(x_{em})\right\| \tag{11}$$

simultaneously for all $x_{em} \in V$, where V is the set of fine model points used for multipoint parameter extraction. This multipoint parameter extraction step differs from (8) in one

important aspect. A perturbation in the fine-model space of Δx_{em} corresponds to a perturbation in the coarse-model space of $B^{(i)}\Delta x_{em}$. This is logical since the matrix $B^{(i)}$ represents the most up-to-date approximation to the mapping between the two spaces. Thus, the available information about the mapping between the two spaces is exploited.

The new extracted coarse model parameters either satisfy the success criterion (10) or they are used to obtain another candidate point which is then added to the set V, and the whole process is repeated (see Fig. 1). This recursive multipoint parameter extraction process is expected to improve the uniqueness of the extraction step. This may lead to the satisfaction of the success criterion (10) or the step is declared a failure. Failure is declared in one of two cases: either the vector of extracted parameters approaches a limiting value with the success criterion not satisfied, or the number of fine model simulations since the last successful iteration has reached $n + 1$. In the first case, the extracted coarse model parameters are trusted and the accuracy of the linearization used to predict $h^{(i)}$ is suspected. Thus, to ensure a successful step from the current point $x_{em}^{(i)}$, the trust region size is shrunk and a new suggested point $x_{em}^{(i+1)}$ is obtained. In the latter case, sufficient information is available to obtain an estimate
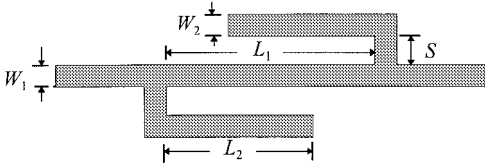
Fig. 2. The DFS filter [5].

for the Jacobian of the fine-model responses with respect to the fine-model parameters. This is done by solving the system of linear equations

$$\begin{pmatrix} \left(x_{em}^{(i)} - x_{em}^{(i+1)}\right)^T \\ \left(x_{em}^{(i)} - x_t^{(1)}\right)^T \\ \vdots \\ \left(x_{em}^{(i)} - x_t^{(n-1)}\right)^T \end{pmatrix} J^T = \begin{pmatrix} \left(g^{(i)} - g^{(i+1)}\right)^T \\ \left(g^{(i)} - g_t^{(1)}\right)^T \\ \vdots \\ \left(g^{(i)} - g_t^{(n-1)}\right)^T \end{pmatrix} \quad (12)$$

where $x_t^{(k)}$ is the kth candidate point used for multipoint parameter extraction and $g_t^{(k)}$ is the corresponding error between the fine-model response and the optimal coarse-model response. This matrix is then used to obtain a step $h^{(i)}$ in the parameter space by solving the system of equations

$$\left(J^T J + \lambda I\right) h^{(i)} = -J^T g^{(i)} \quad (13)$$

varying the parameter λ until $\|h^{(i)}\| \leq \delta$. If there is no reduction in the l_2 norm of the vector function g, the trust region is shrunk and (13) is resolved. This is repeated until either the size of the trust region has shrunk significantly and hence the algorithm terminates or a successful step is taken. The successful step is then used instead of the step obtained by (9).

At the end of each iteration, the ratio between the actual reduction in the l_2 norm of the vector f and the predicted reduction using linearization is used to check the accuracy of the linearization. The criterion

$$\left(\left\|f^{(i)}\right\| - \left\|f^{(i+1)}\right\|\right) \geq 0.80 \left(\left\|f^{(i)}\right\| - \left\|f^{(i)} + B^{(i)} h^{(i)}\right\|\right) \quad (14)$$

was used to check how accurate the linearization is. If (14) is satisfied then we exploit the accuracy of the linearization and increase the size of the trust region.

In the initialization phase we assign $x_{em}^{(0)} = x_{os}^*$ and $B^{(0)} = I$, the identity matrix. Also, we assign values to the two parameters δ_f and ε. These two parameters are used to determine the termination condition of the algorithm.

As there is no iteration prior to the first iteration, we are not able to compare the norm of f with a previous value to ensure the uniqueness of the step. To ensure the uniqueness of $f^{(0)}$, the multipoint parameter extraction at the first point is repeated for an increasing number of points in the set V until it approaches a limiting value. This limiting value can then be trusted and the algorithm proceeds. For any iteration $i \geq 0$, the basic steps taken are as follows.

TABLE I
MATERIAL AND PHYSICAL PARAMETERS FOR THE
COARSE AND FINE *em* MODELS OF THE DFS FILTER

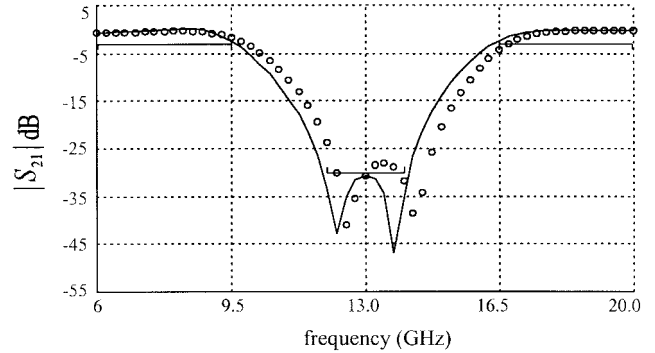| Model Parameter	Value
substrate dielectric constant	9.9
substrate thickness (mil)	5
shielding cover height (mil)	∞
conducting material thickness	3.0E-6
substrate dielectric loss tangent	2.0E-3
resistivity of metal (Ωm)	1.72E-8
magnetic loss tangent	0
surface reactance (Ω/sq)	0
lower frequency limit (GHz)	5
upper frequency limit (GHz)	20
frequency increment size (GHz)	0.25

Fig. 3. The optimal coarse model response (———) and the fine model response (∘) at the starting point for the DFS filter.

TABLE II
VALUES OF OPTIMIZABLE PARAMETERS AT EACH ITERATION FOR THE DFS FILTER

Parameter	$x_{em}^{(0)}$	$x_{em}^{(1)}$	$x_{em}^{(2)}$
L_1	88.8	89.5	94.3
L_2	84.1	84.6	85.4
S	3.9	4.7	4.7
all values are in mils			

TRASM Algorithm

Step 0: Given $x_{em}^{(i)}, f^{(i)}, B^{(i)}$ and $\delta^{(i)}$. Set $\delta^{(i+1)} = \delta^{(i)}$.

Step 1: Obtain $h^{(i)}$ by solving (9) with $\delta = \delta^{(i+1)}$. Let $\delta^{(i+1)} = \|h^{(i)}\|_2$.

Step 2: If $\delta^{(i+1)} \leq \delta_f$ stop else evaluate $x_{em}^{(i+1)}$ using (5) and set $V = \{x_{em}^{(i+1)}\}$.

Step 3: Apply multipoint parameter extraction using the points in the set V to obtain $f^{(i+1)}$.

Step 4: If the success criterion (10) is satisfied go to Step 9.

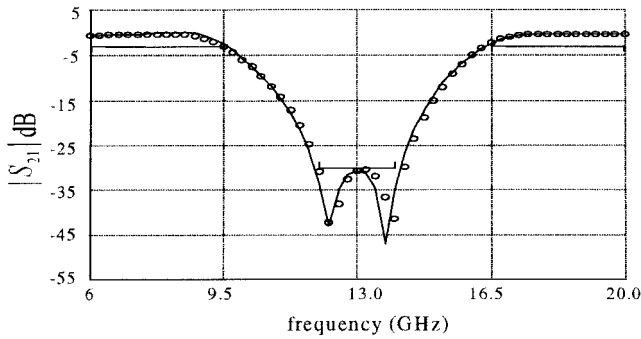*Step 5:* If $|V|$ is equal to one go to Step 8.

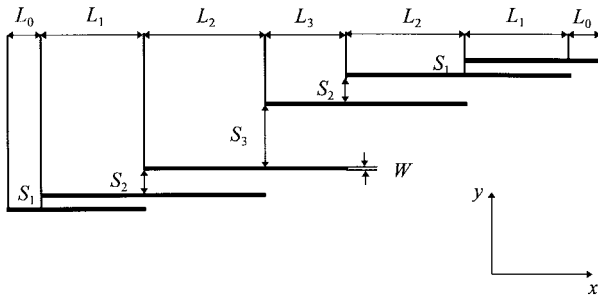Fig. 4.   The optimal coarse model response (———) and the final fine model response (∘) for the DFS filter.

Fig. 5.   The structure of the HTS filter [1], [7].

Comment: $|V|$ denotes the cardinality of the set V.

Step 6:   Compare $f^{(i+1)}$ obtained using $|V|$ fine-model points with that previously obtained using $|V| - 1$ fine-model points. If $f^{(i+1)}$ is approaching a limiting value, shrink the trust region size $\delta^{(i+1)}$ and go to Step 1.

Step 7:   If $|V|$ is equal to n, obtain an approximation for the Jacobian of the fine-model responses, shrink the trust region size $\delta^{(i+1)}$, evaluate a new step $h^{(i)}$ by solving (13) with $\delta = \delta^{(i+1)}$ for a suitable value of λ that results in the reduction in the l_2 norm of the vector g and go to Step 2.

Comment: The trust region is shrunk to ensure a successful step.

Step 8:   Obtain a temporary point using $x_{em}^{(i+1)}$, $f^{(i+1)}$, and $\delta^{(i+1)}$. Add this point to the set V and go to Step 3.

Step 9:   Update the matrix $B^{(i)}$ to $B^{(i+1)}$ using Broyden's formula [4].

Step 10:   If $\|R_{em}(x_{em}^{(i+1)}) - R_{em}(x_{em}^{(i)})\| \leq \varepsilon$ stop.

Step 11:   Increase the trust region size $\delta^{(i+1)}$ if (14) is satisfied.

Step 12:   Let $i = i + 1$. Go to Step 0.

The algorithm terminates if the size of the trust region $\delta^{(i+1)}$ has shrunk below a certain threshold or if there is no significant change in the fine model responses in two consecutive iterations. The algorithm produces two main results. These results are the final fine-model design $\overline{x}_{em}$ and the matrix B which represents the mapping between the two spaces.

In our implementation, proper scaling is applied to the optimizable parameters to make them of the same order. The

TABLE III
MATERIAL AND PHYSICAL PARAMETERS FOR THE HTS FILTER

| Model Parameter	OSA90/hope	*em*
substrate dielectric constant	23.425	23.425
substrate thickness (mil)	19.9516	19.9516
shielding cover height (mil)	∞	250
conducting material thickness	1.968E-2	0
substrate dielectric loss tangent	3.0E-5	3.0E-5
resistivity of metal (Ωm)	0	4.032E-8
surface roughness of metal	0	—
magnetic loss tangent	—	0
surface reactance (Ω/sq)	—	0
x-grid cell size (mil)	—	1.00
y-grid cell size (mil)	—	1.75
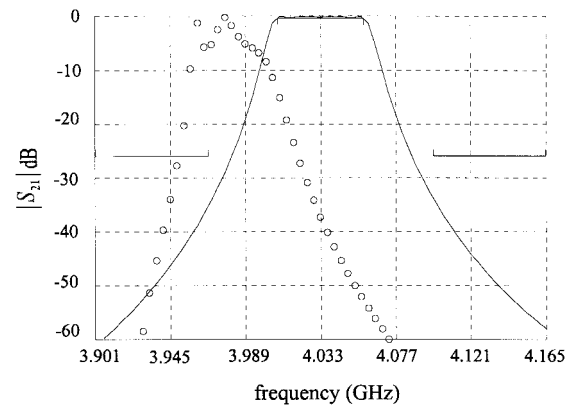
Fig. 6.   The optimal coarse model response (—) and the fine model response (∘) at the starting point for the HTS filter.
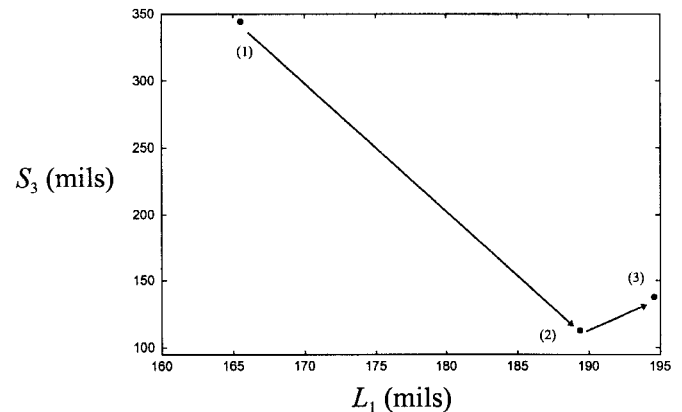

Fig. 7.   The variation of two of the extracted coarse model parameters in the first iteration with the number of points used for parameter extraction where (1) is obtained using a single fine-model point, (2) is obtained using two fine-model points, and (3) is obtained using three fine-model points.

initial trust region size is taken as 2% to 10% of the l_∞ norm of the vector of scaled parameters.

V.   EXAMPLES

Double-Folded Stub Filter

We consider the design of the double-folded stub (DFS) microstrip structure shown in Fig. 2 [5]. Folding the stubs
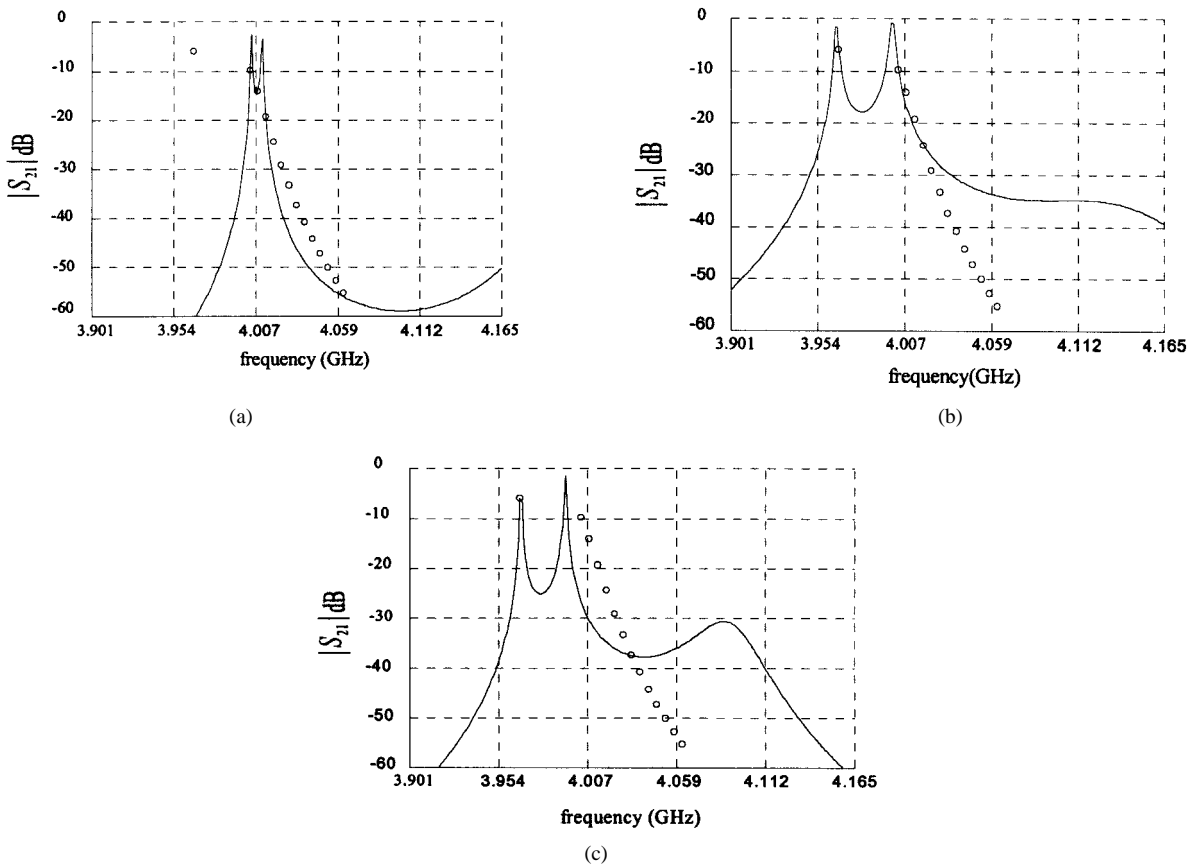
Fig. 8. The coarse model response (—) and the fine model response (○) corresponding to the three extracted points in Fig. 7 where (a) is obtained using a single fine-model point, (b) is obtained using two fine-model points, and (c) is obtained using three fine-model points.

reduces the filter area w.r.t. the conventional double-stub structure [6]. The filter is characterized by five parameters: W_1, W_2, S, L_1, and L_2 (see Fig. 2). L_1, L_2, and S are chosen as optimization variables. W_1 and W_2 are fixed at 4.8 mil. The design specifications are given by $|S_{21}| \geq -3$ dB in the passband and $|S_{21}| \leq -30$ dB in the stopband, where the passband includes frequencies below 9.5 GHz and above 16.5 GHz and the stopband lies in the range [12 GHz, 14 GHz]. The structure is simulated by Sonnet's *em* through Empipe. The coarse model is a coarse-grid *em* model with cell size 4.8 mil by 4.8 mil. The fine model is a fine-grid *em* model with cell size 1.6 mil by 1.6 mil. Other parameters are summarized in Table I.

Fig. 3 shows the optimal coarse-model response along with the fine-model *em* response evaluated using the optimal coarse-model parameters. The time needed to simulate the structure (coarse model) at a single frequency is only 5 CPU seconds on a Sun SPARCstation 10. This includes automatic response interpolation carried out to accommodate off-grid geometries.

It is clear from Fig. 3 that the fine-model response violates the design specifications at the starting point. The new ASM algorithm required only two iterations to reach the final design. The algorithm's progress is shown in Table II. The number of fine-model points needed is five. Linear response interpolation was enabled to simulate the off-grid fine-model points. The response of the fine-model at the final design is

shown in Fig. 4. The CPU time needed for the fine model is approximately 70 s per frequency point.

HTS Filter

We consider optimization of an HTS filter [1], [7]. This filter is illustrated in Fig. 5. The specifications are $|S_{21}| \geq 0.95$ in the passband and $|S_{21}| \leq 0.05$ in the stopband, where the stopband includes frequencies below 3.967 GHz and above 4.099 GHz, and the passband lies in the range [4.008 GHz, 4.058 GHz]. The design variables for this problem are L_1, L_2, L_3, S_1, S_2, and S_3. We take $L_0 = 50$ mil and $W = 7$ mil. The coarse model exploits the empirical models of microstrip lines, coupled lines, and open stubs available in OSA90/hope. The fine model employs a fine-grid *em* simulation. The material and physical parameters values used in both OSA90/hope and in *em* are shown in Table III. The coarse model is first optimized using the OSA90/hope minimax optimizer. The fine-model response at the optimal coarse-model design is shown in Fig. 6. The parameter extraction for this problem has several solutions. Fig. 7 shows how two of the extracted coarse-model parameters changed with the number of points used for parameter extraction in the first iteration. The first point (1) is obtained using normal parameter extraction. These extracted values would have caused the original ASM technique to diverge. The new technique automatically generates a candidate point which is then used together with the original point to carry out a
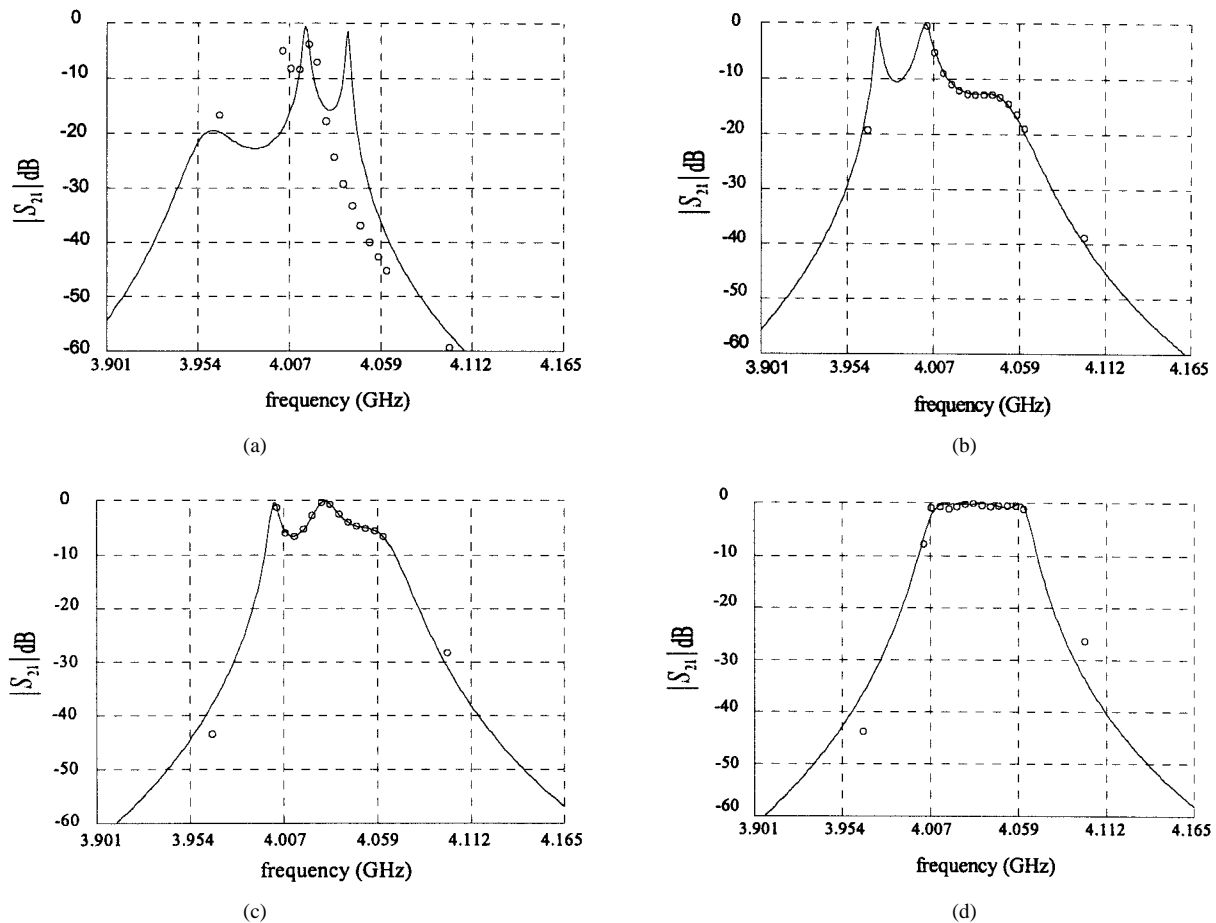
Fig. 9.   The coarse-model response (—) at the extracted point and the fine-model response (o) corresponding to the second, third, fourth, and fifth iterations.

TABLE IV
INITIAL AND FINAL DESIGNS OF THE FINE MODEL FOR THE HTS FILTER

Parameter	$x_{em}^{(0)}$	$x_{em}^{(5)}$
L_1	188.33	181.43
L_2	197.98	200.51
L_3	188.58	180.49
S_1	21.97	19.44
S_2	99.12	80.52
S_3	111.67	83.41
all values are in mils		

Fig. 10.   The optimal coarse-model response (—) and the final fine-model response (o) for the HTS filter.

two-point parameter extraction, and the second point (2) is obtained. To confirm that this point is the required one, a third candidate point is automatically generated and the extraction is repeated using the three points to obtain the third extracted point (3). The second and third extracted points show that the extracted vector of coarse model parameters is approaching a limiting value and can thus be trusted. The coarse model responses corresponding to the three extracted points of Fig. 7 are shown in Fig. 8.

For the remaining iterations, single-point parameter extraction worked well. The fine-model responses and the coarse-model responses for the corresponding extracted points are shown in Fig. 9. The final fine-model design was obtained
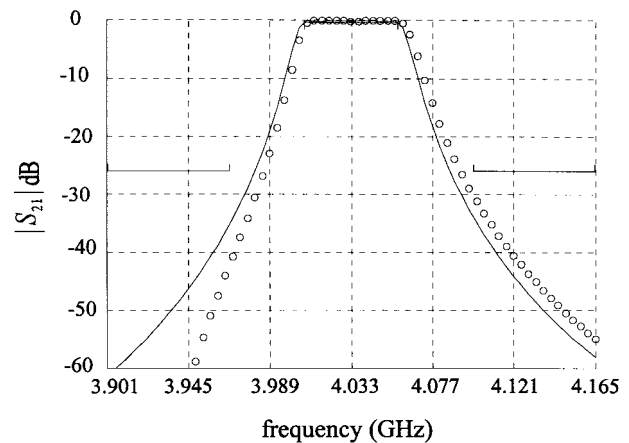
in five iterations which required eight fine-model simulations. The final fine-model design is given in Table IV. The fine-model response at this design is shown in Fig. 10. The passband ripples are shown in Fig. 11.

In the original space mapping approaches [1], [7], this example required significant manual intervention to successfully complete the parameter extraction phase. Furthermore, without such intervention the previous approaches would not work.

TABLE V
VALUES OF OPTIMIZABLE PARAMETERS AT EACH ITERATION OF THE NEW ASM TECHNIQUE
FOR THE TWO-SECTION WAVEGUIDE TRANSFORMER USING TWO ANALYTICAL MODELS

Parameter	$x_{em}^{(0)}$	$x_{em}^{(1)}$	$x_{em}^{(2)}$	$x_{em}^{(3)}$
b_1	0.712	0.715	0.716	0.716
b_2	1.395	1.400	1.402	1.402
L_1	1.657	1.591	1.560	1.560
L_2	1.590	1.541	1.518	1.518
all values are in cm				

TABLE VI
VALUES OF OPTIMIZABLE PARAMETERS AT EACH ITERATION OF THE NEW ASM TECHNIQUE FOR THE
TWO-SECTION WAVEGUIDE TRANSFORMER USING MAXWELL EMINENCE AND AN IDEAL ANALYTICAL MODEL

Parameter	$x_{em}^{(0)}$	$x_{em}^{(1)}$	$x_{em}^{(2)}$	$x_{em}^{(3)}$
b_1	0.712	0.713	0.719	0.716
b_2	1.395	1.397	1.408	1.402
L_1	1.657	1.595	1.565	1.567
L_2	1.590	1.535	1.517	1.517
all values are in cm				

TABLE VII
VALUES OF OPTIMIZABLE PARAMETERS AT EACH ITERATION OF THE NEW ASM TECHNIQUE
FOR THE THREE-SECTION WAVEGUIDE TRANSFORMER USING TWO ANALYTICAL MODELS

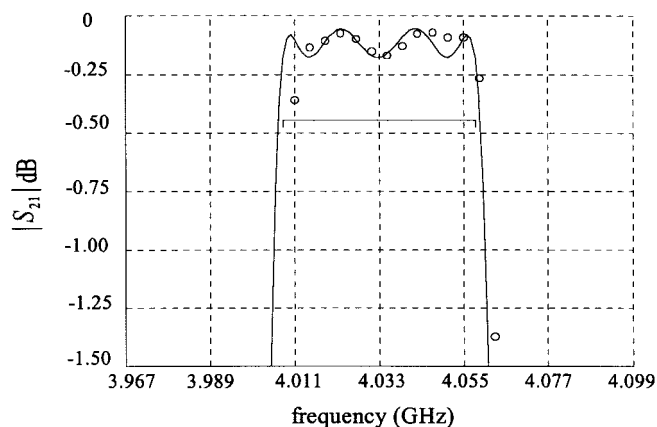| Parameter	$x_{em}^{(0)}$	$x_{em}^{(1)}$	$x_{em}^{(2)}$	$x_{em}^{(3)}$	$x_{em}^{(4)}$
b_1	0.903	0.905	0.881	0.891	0.892
b_2	1.371	1.363	1.298	1.325	1.325
b_3	1.736	1.718	1.692	1.701	1.702
L_1	1.549	1.500	1.500	1.489	1.489
L_2	1.584	1.575	1.575	1.575	1.577
L_3	1.646	1.768	1.880	1.853	1.850
all values are in cm					

Fig. 11. The optimal coarse-model response (—) and the final fine-model response (○) for the HTS filter in the passband.
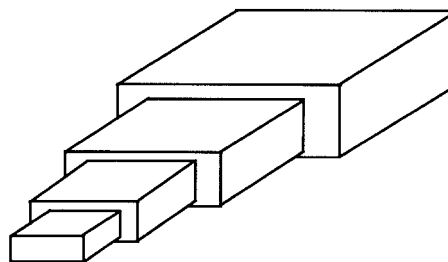

Fig. 12. A typical two-section waveguide transformer.

Waveguide Transformers

Three designs of two-, three-, and seven-section waveguide transformers were considered. The two-section waveguide transformer is shown in Fig. 12. These examples are classical microwave circuit design problems [8]. Two different sets of
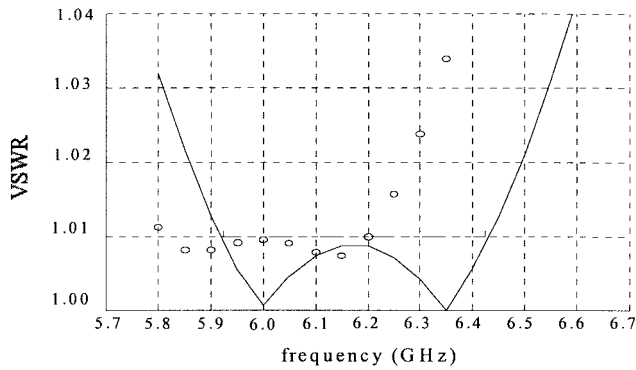
Fig. 13. The optimal response of the ideal analytical model (—) and the response of the nonideal analytical model (○) at the starting point for the two-section waveguide transformer.

Fig. 14. The optimal response of the ideal analytical model (—) and the final response of the nonideal analytical model (○) for the two-section waveguide transformer.

Fig. 15. The optimal response of the ideal analytical model (—) and the response of Maxwell Eminence (○) at the starting point for the two-section waveguide transformer.
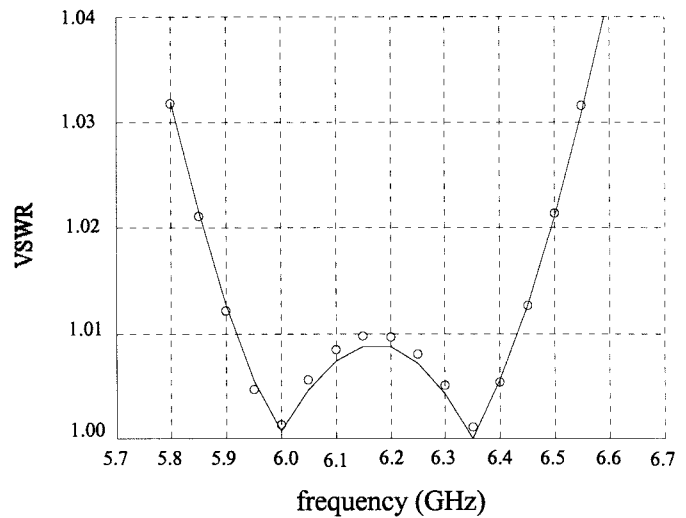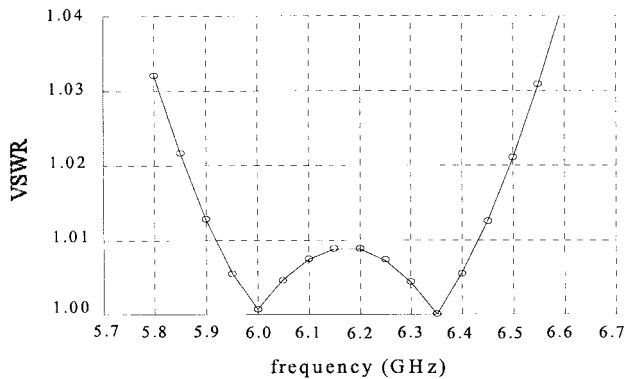

Fig. 16. The optimal response of the ideal analytical model (—) and the final Maxwell Eminence response (○) for the two-section waveguide transformer.
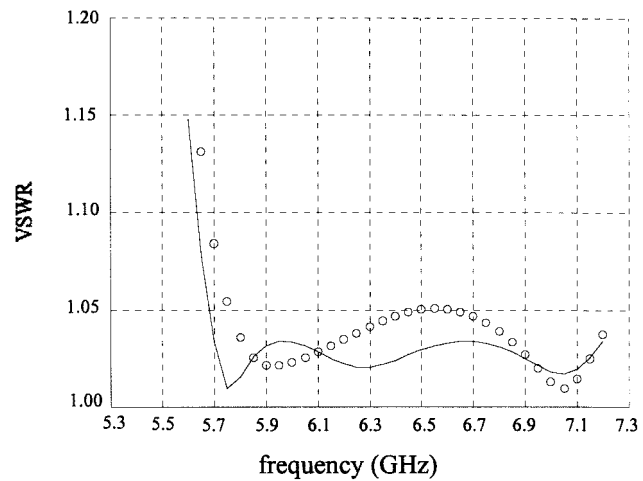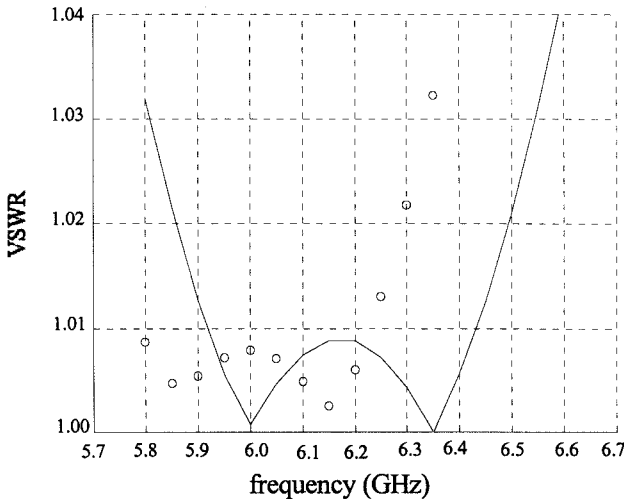

Fig. 17. The optimal response of the ideal analytical model (—) and the response of the nonideal analytical model (○) at the starting point for the three-section waveguide transformer.

The designable parameters for these design problems are the height and length of each waveguide section.

The two-section transformer is optimized using the two analytical models. The optimum ideal model response is shown in Fig. 13 along with the nonideal model response at the same point. Our algorithm terminated in three iterations, requiring five fine-model simulations. The final nonideal model design is given in Table V. The corresponding nonideal model response is shown in Fig. 14. This example is known to have more than one minimum for the parameter extraction step [2]. However, our new algorithm converged successfully. The number of simulations needed to align the two models is smaller than that reported in [2]. The same transformer is then optimized using Maxwell Eminence and the ideal analytical model. Nine adaptive passes were allowed for Maxwell Eminence with allowable delta S set to 0.0001. The initial fine-model response is shown in Fig. 15. The final design was obtained in three iterations which required five Maxwell Eminence fine-model simulations. This is one half the number of fine-model

models were used. The first set exploits two empirical models: an "ideal" analytical model which neglects the junction discontinuity and a more accurate "nonideal" analytical model which includes the junction discontinuity effects [8]. The second set uses the ideal analytical model of the first set as the coarse model while Maxwell Eminence is used as the fine model.
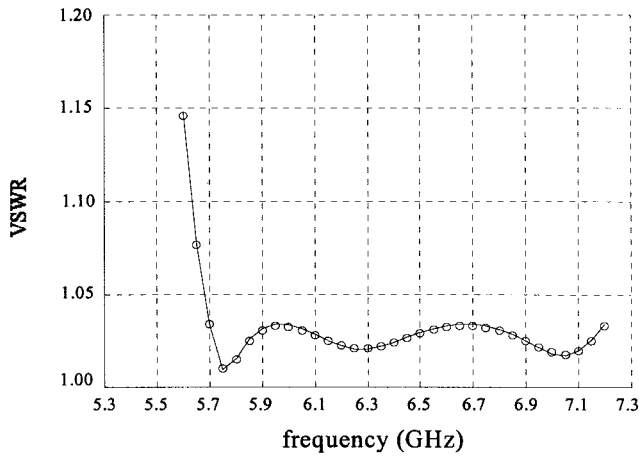
Fig. 18.   The optimal response of the ideal analytical model (—) and the final response of the nonideal analytical model (○) for the three-section waveguide transformer.
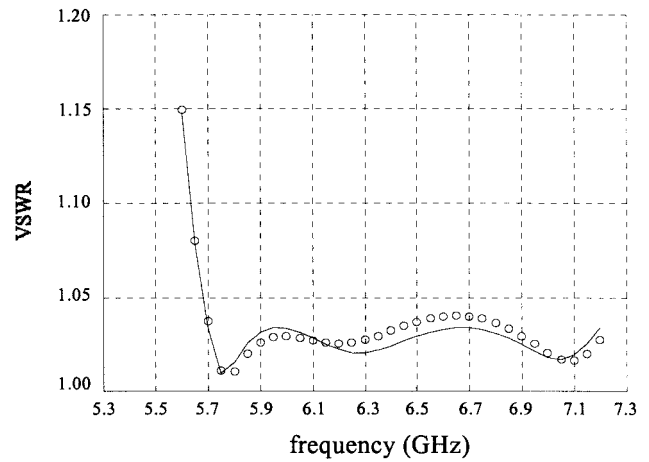

Fig. 20.   The optimal response of the ideal analytical model (—) and the final Maxwell Eminence response (○) for the three-section waveguide transformer.
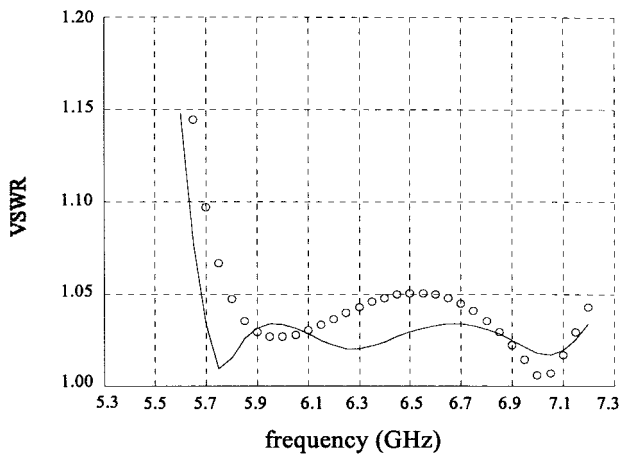

Fig. 19.   The optimal response of the ideal analytical model (—) and the response of Maxwell Eminence (○) at the starting point for the three-section waveguide transformer.
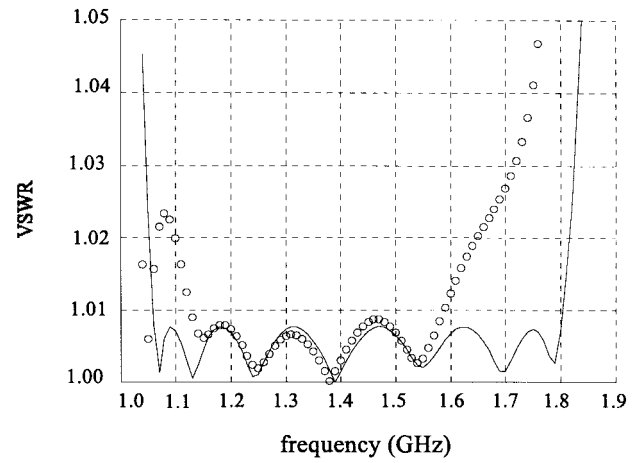

Fig. 21.   The optimal ideal analytical model response (—) and the response of the nonideal analytical model (○) at the starting point for the seven-section waveguide transformer.

TABLE VIII
VALUES OF OPTIMIZABLE PARAMETERS AT EACH ITERATION OF THE NEW
ASM TECHNIQUE FOR THE THREE-SECTION WAVEGUIDE TRANSFORMER
USING MAXWELL EMINENCE AND AN IDEAL ANALYTICAL MODEL

Parameter	$x_{em}^{(0)}$	$x_{em}^{(1)}$	$x_{em}^{(2)}$
b_1	0.903	0.898	0.893
b_2	1.371	1.340	1.327
b_3	1.736	1.707	1.703
L_1	1.549	1.514	1.495
L_2	1.584	1.566	1.568
L_3	1.646	1.810	1.848
all values are in cm			

Fig. 22.   The optimal response of the ideal analytical model (—) and the final response of the nonideal analytical model (○) for the seven-section waveguide transformer.

simulations reported in [2]. The Maxwell Eminence fine-model design is shown in Table VI and the corresponding fine-model response is shown in Fig. 16.

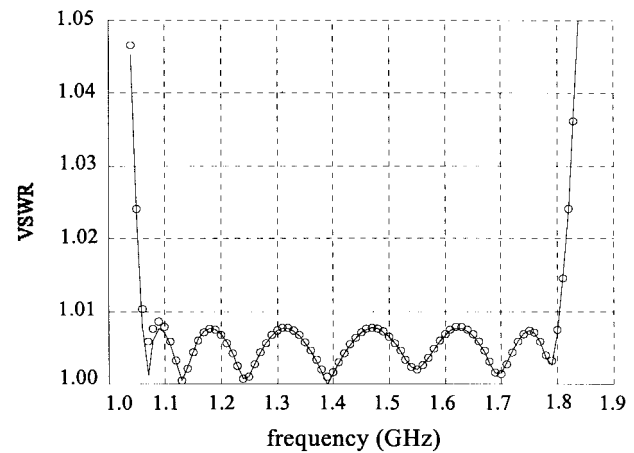The previous steps were repeated for the three-section waveguide transformer. The initial fine-model response is shown in Fig. 17. Using the two analytical models, the final design was obtained in four iterations which required six fine-model simulations. This final design is shown in Table VII.

TABLE IX
VALUES OF OPTIMIZABLE PARAMETERS AT THE INITIAL
AND FINAL DESIGN FOR THE SEVEN-SECTION WAVEGUIDE
TRANSFORMER USING TWO ANALYTICAL MODELS

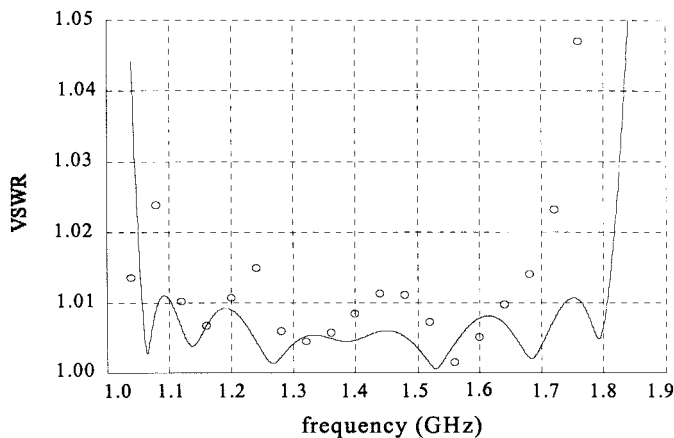| Parameter	$x_{em}^{(0)}$	$x_{em}^{(3)}$
b_1	7.86732	7.87152
b_2	6.61888	6.64855
b_3	4.68540	4.74039
b_4	2.91987	2.96613
b_5	1.81412	1.83659
b_6	1.27658	1.28401
b_7	1.06847	1.06967
L_1	7.10588	7.24590
L_2	7.12201	7.08753
L_3	7.11760	6.91817
L_4	7.12331	6.90979
L_5	7.12815	6.98383
L_6	7.12154	7.03845
L_7	7.12945	7.07431

all values are in cm

Fig. 23. The optimal response of the ideal analytical model (—) and the response of Maxwell Eminence ($\circ$) at the starting point for the seven-section waveguide transformer.

Fig. 24. The optimal response of the ideal analytical model (—) and the final Maxwell Eminence response ($\circ$) for the seven-section waveguide transformer.

TABLE X
VALUES OF OPTIMIZABLE PARAMETERS AT THE INITIAL AND FINAL
DESIGN FOR THE SEVEN-SECTION WAVEGUIDE TRANSFORMER
USING MAXWELL EMINENCE AND AN IDEAL ANALYTICAL MODEL

Parameter	$x_{em}^{(0)}$	$x_{em}^{(3)}$
b_1	7.86732	7.87494
b_2	6.61888	6.65247
b_3	4.68540	4.74347
b_4	2.91987	2.97030
b_5	1.81412	1.84134
b_6	1.27658	1.28891
b_7	1.06847	1.07201
L_1	7.10588	7.18744
L_2	7.12201	7.03537
L_3	7.11760	6.89166
L_4	7.12331	6.89697
L_5	7.12815	6.98825
L_6	7.12154	7.05869
L_7	7.12945	7.12572

all values are in cm

The corresponding fine-model response is indistinguishable from the optimal coarse-model response as shown in Fig. 18.

The design of the three-section transformer is then repeated using Maxwell Eminence and the ideal analytical model. We allowed only five adaptive passes with the same value of allowable delta S as before. The initial Maxwell Eminence fine-model response is shown in Fig. 19. The algorithm terminated in two iterations with a total number of nine fine-model simulations. Most of these fine-model simulations were used to shrink the trust region around the final design. The final design is shown in Table VIII. The corresponding Maxwell Eminence fine-model response is shown in Fig. 20.

The design of a seven-section waveguide transformer was also considered. The designable parameters for this problem are the height and lengt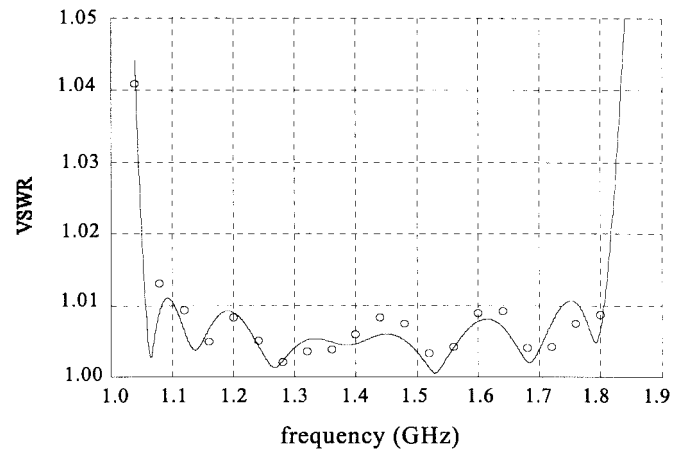h of each waveguide section. Using the two analytical models, the final design was obtained in three iterations which required six fine-model simulations. The initial fine-model response is shown in Fig. 21. The fine-model response corresponding to the final design is almost identical to the optimal coarse-model response as shown in Fig. 22. Table IX shows the final fine model design.

Finally, the design of the seven-section transformer was carried out using Maxwell Eminence and an ideal analytical model. We allowed ten refinement passes with allowable delta S of 0.001. The algorithm terminated in three iterations which required 11 Maxwell Eminence fine-model simulations. The initial Maxwell Eminence response is shown in Fig. 23. The final fine-model response is shown in Fig. 24. Table X shows the corresponding Maxwell Eminence fine model design.
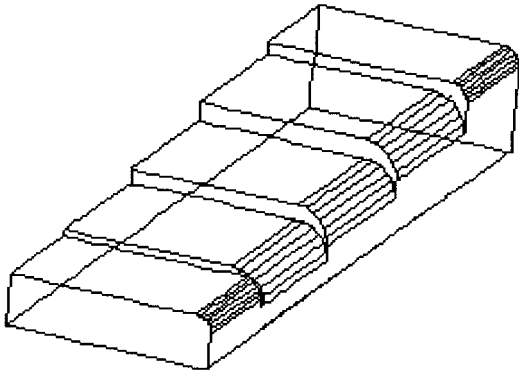
Fig. 25. The simulated part of the three-section waveguide transformer with rounded corners [9].

A Three-Section Waveguide Transformer with Rounded Corners [9]

In this example, we considered the design of a three-section transformer with rounded corners. The designable parameters for this problem are the height and length of each waveguide section. The specifications are $|S_{11}| \leq -30$ dB for a range of frequencies extending from 9.5 to 15 GHz. The fine model of this circuit exploits HP HFSS. The coarse model exploits an ideal empirical model that does not take into account the rounding of the corners. One quadrant of the transformer is shown in Fig. 25. We exploited the geometrical symmetry of the problem to reduce the required CPU time of HP HFSS.

Each time a new HP HFSS simulation is requested by the algorithm, a new project is created using the new values for the length and height of each section. To facilitate this process, a MATLAB[5] program was developed that converts the values of the designable parameters into the corresponding HP HFSS drawing commands with the appropriate values. This approach accelerates the generation of new HP HFSS projects and eliminates the possibility of wrong dimensions.

The initial response of the fine model at the optimal coarse-model design is shown in Fig. 26. Clearly, the specifications are slightly violated at this point. Only one iteration was needed to reach the final fine-model design. The required number of HP HFSS simulations is seven. The first three of these simulations were needed to trust the parameter extraction at the first point. The other fine-model points were needed to contract the size of the trust region to the termination size. The final HP HFSS fine-model design is given in Table XI. The corresponding fine-model response is shown in Fig. 27.

VI. MONTE CARLO ANALYSIS USING SPACE MAPPING [5]

The final $\boldsymbol{B}$ matrix obtained by the algorithm represents the best available information about the mapping between the two spaces. A perturbation of $\Delta\boldsymbol{x}_{em}$ in the fine-model space is mapped to a perturbation of $\Delta\boldsymbol{x}_{os}$ in the coarse-model space by

$$\Delta\boldsymbol{x}_{os} = B\Delta\boldsymbol{x}_{em}. \tag{15}$$

The perturbations in the coarse-model space and fine-model space are with respect to $\boldsymbol{x}_{os}^*$ and $\overline{\boldsymbol{x}}_{em}$, respectively. The
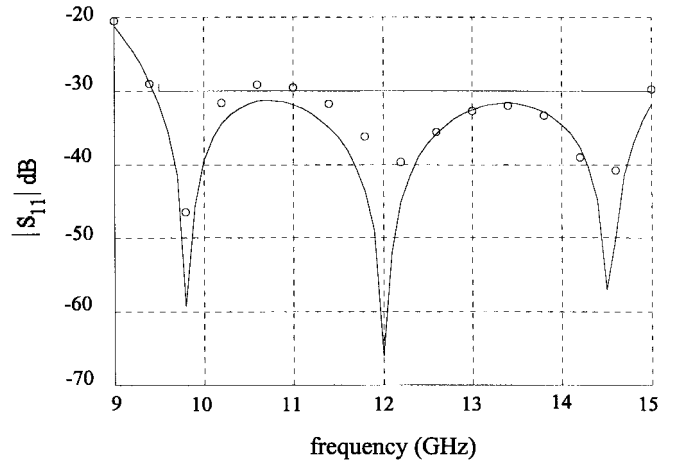
Fig. 26. The optimal response of the ideal analytical model (—) and the response of HP HFSS (○) at the starting point for the three-section waveguide transformer with rounded corners.

TABLE XI
VALUES OF OPTIMIZABLE PARAMETERS AT EACH ITERATION OF THE NEW ASM TECHNIQUE FOR THE THREE-SECTION WAVEGUIDE TRANSFORMER WITH ROUND CORNERS USING HP HFSS AND AN IDEAL ANALYTICAL MODEL

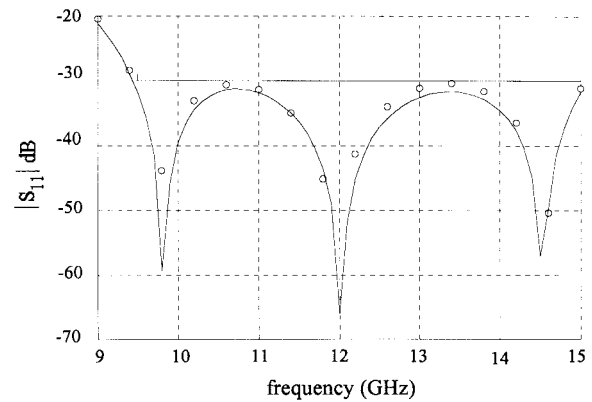| Parameter	$x_{em}^{(0)}$	$x_{em}^{(1)}$
b_1	0.33276	0.32971
b_2	0.26551	0.26396
b_3	0.21186	0.20978
L_1	0.32556	0.33208
L_2	0.32640	0.32335
L_3	0.32556	0.32192
all values are in inch		

Fig. 27. The optimal response of the ideal analytical model (—) and the final HP HFSS response (○) for the three-section waveguide transformer with rounded corners.

established mapping can be used to perform a space-mapped Monte Carlo analysis [5] for the problem under consideration. The random points generated in the fine-model space are mapped to the coarse-model space using (15). Coarse-model simulations are then used instead of the CPU-intensive fine-model simulations. This statistical analysis should enjoy the speed of the coarse model and the accuracy of the fine model.
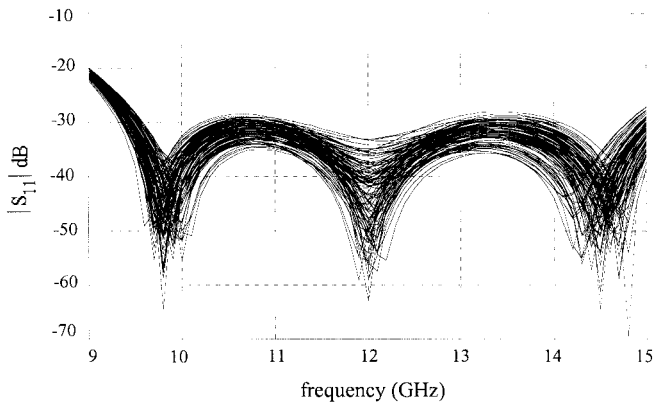
Fig. 28. Monte Carlo analysis for the three-section waveguide transformer with rounded corners assuming 1% uniformly distributed parameters.
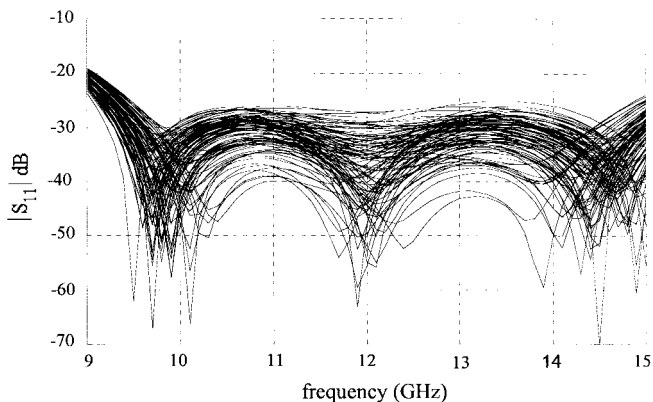

Fig. 29. Monte Carlo analysis for the three-section waveguide transformer with rounded corners assuming 2% uniformly distributed parameters.
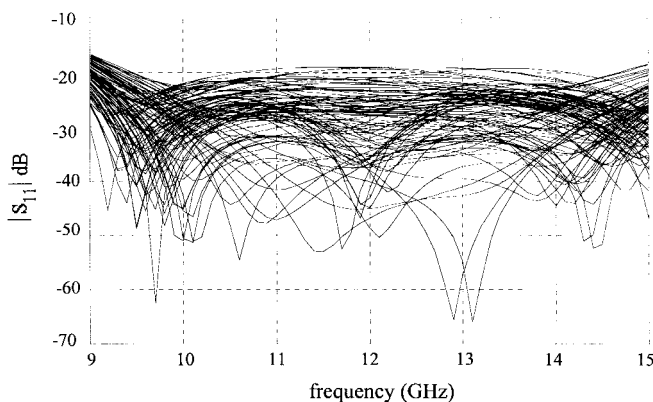

Fig. 30. Monte Carlo analysis for the three-section waveguide transformer with rounded corners assuming 5% uniformly distributed parameters.

To demonstrate this approach, we carried out a Monte Carlo analysis of the three-section waveguide transformer with rounded corners. The fine-model parameters were assumed to be uniformly distributed with tolerances of 1, 2, and 5%. The corresponding responses are shown in Figs. 28–30. The estimated yields for these tolerances are 39, 4, and 0%.

VII. CONCLUSIONS

A powerful new algorithm implementing the aggressive space mapping technique is introduced. The new algorithm, TRASM, automatically improves the uniqueness of the parameter extraction step, the most critical step in the space mapping process, and exploits all available fine-model simulations. Also, the proposed algorithm integrates the trust region concept with the original ASM technique. Through examples which have proved difficult in the past, we show that the TRASM algorithm automatically overcomes the nonuniqueness of the parameter extraction step in a logical way. The results show that very few EM simulations are needed to reach the final design. We showed also how the established mapping between the two spaces can be used to carry out a space-mapped Monte Carlo analysis of the fine model.

REFERENCES

[1] J. W. Bandler, R. M. Biernacki, S. H. Chen, R. H. Hemmers, and K. Madsen, "Electromagnetic optimization exploiting aggressive space mapping," *IEEE Trans. Microwave Theory Tech.*, vol. 43, pp. 2874–2882, 1995.
[2] J. W. Bandler, R. M. Biernacki, and S. H. Chen, "Fully automated space mapping optimization of 3D structures," in *IEEE MTT-S Int. Microwave Symp. Dig.*, San Francisco, CA, 1996, pp. 753–756.
[3] J. J. Moré and D. C. Sorenson, "Computing a trust region step," *SIAM J. Sci. Stat. Comp.*, vol. 4, pp. 553–572, 1983.
[4] C. G. Broyden, "A class of methods for solving nonlinear simultaneous equations," *Math. Comp.*, vol. 19, pp. 577–593, 1965.
[5] J. W. Bandler, R. M. Biernacki, S. H. Chen, P. A. Grobelny, and R. H. Hemmers, "Space mapping technique for electromagnetic optimiztion," *IEEE Trans. Microwave Theory Tech.*, vol. 42, pp. 2536–2544, 1994.
[6] J. C. Rautio, private communication, 1992.
[7] J. W. Bandler, R. M. Biernacki, S. H. Chen, W. J. Gestinger, P. A. Grobelny, C. Moskowitz, and S. H. Talisa, "Electromagnetic design of high-temperature superconducting filters," *Int. J. Microwave and Millimeter-Wave CAE*, vol. 5, pp. 331–343, 1995.
[8] J. W. Bandler, "Computer optimization of inhomogeneous waveguide transformers," *IEEE Trans. Microwave Theory Tech.*, vol. MTT-17, pp. 563–571, 1969.
[9] *Empipe3D*^{TM} *Manual*, Version 4.0, formerly Optimization Systems Associates Inc., Dundas, Ont., Canada, L9H 5E7, 1997, Chapter 5, now HP EEsof Division, Santa Rosa, CA 95403.

Mohamed H. Bakr (S'98) was born in Cairo, Egypt, on November 7, 1969. He received the B.Sc. degree in electronics and communications engineering from Cairo University, Egypt, in 1992 with distinction (honors). In 1996 he received the Masters degree in engineering mathematics from Cairo University.

In October 1992, he joined the Department of Engineering Mathematics and Physics, Faculty of Engineering, Cairo University. He joined the Department of Electrical and Computer Engineering, McMaster University, Hamilton, Ont., Canada in September 1996, where he is currently a Ph.D. student. His research is carried out in the Simulation Optimization Systems Research Laboratory. During the 1997/1998 academic year, he held a student internship from the Telecommunications Research Institute of Ontario to work at Optimization Systems Associates, Inc. He is interested in optimization methods, computer-aided design of microwave circuits, and neural networks.

Mr. Bakr currently holds an Ontario Graduate Scholarship.
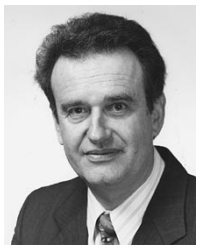
John W. Bandler (S'66–M'66–SM'74–F'78) was born in Jerusalem, on November 9, 1941. He studied at Imperial College of Science and Technology, London, England, from 1960 to 1966. He received the B.Sc.(Eng.), Ph.D., and D.Sc.(Eng.) degrees from the University of London, London, England, in 1963, 1967 and 1976, respectively.

He joined Mullard Research Laboratories, Redhill, Surrey, England in 1966. From 1967 to 1969 he was a Postdoctorate Fellow and Sessional Lecturer at the University of Manitoba, Winnipeg, Canada. He joined McMaster University, Hamilton, Canada, in 1969, where he is currently Professor of Electrical and Computer Engineering. He has served as Chairman of the Department of Electrical Engineering and Dean of the Faculty of Engineering. He currently directs research in the Simulation Optimization Systems Research Laboratory. He is a member of the Micronet Network of Centres of Excellence. He was President of Optimization Systems Associates Inc. (OSA), which he founded in 1983, until November 20, 1997, the date of acquisition of OSA by Hewlett-Packard Company (HP). He is President of Bandler Corporation, which he founded in 1997. He was an Associate Editor of the IEEE TRANSACTIONS ON MICROWAVE THEORY AND TECHNIQUES (1969–1974) and has continued serving as a member of the Editorial Board. He joined the Editorial Boards of the *International Journal of Numerical Modeling* in 1987, and the *International Journal of Microwave and Millimeterwave Computer-Aided Engineering* in 1989. He has published more than 300 papers from 1965 to 1998.

Dr. Bandler is a fellow of the Royal Society of Canada, a fellow of the Institution of Electrical Engineers (Great Britain), a member of the Association of Professional Engineers of the Province of Ontario (Canada) and a member of the MIT Electromagnetics Academy. He serves as co-chair of the IEEE MTT-S Technical Committee on Computer-Aided Design. He received the Automatic Radio Frequency Techniques Group (ARFTG) Automated Measurements Career Award in 1994.
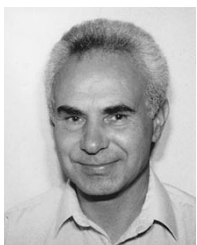
Radoslaw M. Biernacki (M'85–SM'86–F'96) was born in Warsaw, Poland. He received the Ph.D. degree from Warsaw University of Technology in 1976.

He became a Research and Teaching Assistant in 1969 and an Assistant Professor in 1976 at the Institute of Electronics Fundamentals, Warsaw University of Technology, Warsaw, Poland. From 1978 to 1980 he was on leave with the Research Group on Simulation, Optimization and Control and with the Department of Electrical and Computer Engineering, McMaster University, Hamilton, Canada, as a Postdoctorate Fellow. From 1984 to 1986 he was a Visiting Associate Professor at Texas A&M University, College Station. From 1986 to 1997 he was with Optimization Systems Associates Inc., Dundas, Ont., Canada, where he was involved in the development of OSA's commercial CAE software systems and related research. During this period his academic research was carried out in the Simulation Optimization Systems Research Laboratory, McMaster University. In 1997, after acquisition of OSA, he joined the R&D team of HP EEsof. His research in the area of computer-aided engineering has included parameter extraction, statistical device modeling, simulation and optimization, yield-driven design of linear and nonlinear microwave circuits, and electromagnetic design optimization. He has more than 100 publications. He is also an Adjunct Professor in the Department of Electrical and Computer Engineering, McMaster University, Hamilton, Canada.

Shao Hua (Steve) Chen (S'84–M'88–SM'95) was born in Swatow, China. He received the B.S. (Eng.) degree in 1982 from the South China Institute of Technology in Guangzhou, China, and the Ph.D. degree in electrical engineering in 1987 from McMaster University in Hamilton, Ont., Canada.

From July 1982 to August 1983 he was a Teaching Assistant in the Department of Automation at the South China Institute of Technology. During his graduate study at McMaster University from 1983 to 1987, he was awarded an Ontario Graduate Scholarship for two years. He joined Optimization Systems Associates Inc., Dundas, Ont., Canada, in 1987 and has made major contributions to the commercial CAD software development. He has also worked as a Senior Research Engineer in the Simulation Optimization Systems Research Laboratory at McMaster University and engaged in pioneering research on CAD simulation and modeling technology and optimization techniques. In 1997 he joined the Technical Staff at Hewlett-Packard Company, HP EEsof Division. His professional interests include optimization theory and implementation, CAD software architecture, electromagnetic optimization, electronic device modeling, statistical circuit simulation, and computer graphics. He has over 60 technical publications.

Kaj Madsen was born in Denmark in 1943. He received the cand.scient. degree in mathematics from the University of Aarhus in 1968 and the dr.techn. degree from the Technical University of Denmark in 1986.

From 1968 to 1988 he was a Lecturer in Numerical Analysis, apart from the academic year 1973 to 1974, when he was with AERE Harwell, Didcot, England. Most of his career has been spent with the Institute for Numerical Analysis, Technical University of Denmark, but during the years 1981 to 1983 he was with the Computer Science Department, Copenhagen University. During the summer of 1978, he visited McMaster University, Hamilton, Ont., Canada. In 1988 he became Professor with the Institute for Numerical Analysis, Technical University of Denmark. In 1993 he joined the Department of Mathematical Modelling, Technical University of Denmark. During 1988–1993 and since 1995 he has been Head of Department. His fields of interest in teaching and research are parallel algorithms, optimization, and interval analysis.